ADVANCED MATERIALS
www.advmat.de

300-Times-Increased Diffusive Skyrmion Dynamics and Effective Pinning Reduction by Periodic Field Excitation

*Raphael Gruber, Maarten A. Brems, Jan Rothörl, Tobias Sparmann, Maurice Schmitt, Iryna Kononenko, Fabian Kammerbauer, Maria-Andromachi Syskaki, Oded Farago, Peter Virnau, and Mathias Kläui**

Thermally induced skyrmion dynamics, as well as skyrmion pinning effects, in thin films have attracted significant interest. While pinning poses challenges in deterministic skyrmion devices and slows down skyrmion diffusion, for applications in non-conventional computing, both pinning of an appropriate strength and skyrmion diffusion speed are key. Here, periodic field excitations are employed to realize an increase of the skyrmion diffusion by more than two orders of magnitude. Amplifying the excitation, a drastic reduction of the effective skyrmion pinning, is reported, and a transition from pinning-dominated diffusive hopping to dynamics approaching free diffusion is observed. By tailoring the field oscillation frequency and amplitude, a continuous tuning of the effective pinning and skyrmion dynamics is demonstrated, which is a key asset and enabler for non-conventional computing applications. It is found that the periodic excitations additionally allow stabilization of skyrmions at different sizes for field values that are inaccessible in static systems, opening up new approaches to ultrafast skyrmion motion by transiently exciting moving skyrmions.

1. Introduction

Skyrmions are chiral magnetic structures[1–4] that are of major scientific interest as they are promising candidates for various applications in data storage and logic in thin film multilayer systems. The topologically non-trivial magnetic skyrmion texture[3,4] is stabilized by the Dzyaloshinskii–Moriya interaction (DMI) and exhibits quasi-particle properties.[3–6] Hence, the skyrmion can serve as stable information carrier in logic[6–9] and memory[4,10–12] devices. Thereby, tailoring the skyrmion dynamics is a key asset for efficient device operation. For certain devices, deterministic motion is required, which can be realized by a number of mechanisms including external fields, temperature, as well as their gradients,[13–17] and by spin torques generated by currents.[18–26] In the latter case, the skyrmion velocity can be efficiently set by the applied current density. However, skyrmions can also undergo thermally activated diffusion,[6,27–31] which is dependent on temperature and sample-specific material characteristics[6,27,29] and has been lacking means to control the diffusive motion. Thermal diffusion is desired for various applications in non-conventional computing with the performance scaling with the diffusion. Non-conventional computing has recently moved to the focus of research because it enables low-power realizations of complex computing tasks, for which a special need has become apparent in the context of the enormous power consumption of information technology. In case of skyrmions used in Brownian computing concepts,[6,9,29,30,32–34] the energy necessary for the actual computation may predominantly be provided as thermal activation from the surrounding. Specifically, skyrmion diffusion has been employed recently in a Brownian reshuffler[6] as a decorrelation mechanism for probabilistic computing,[6,8,35] but also in Brownian reservoir computing[34] and in Brownian token-based computing.[9,30–32] In all these skyrmion-based computing devices, both operation speed and energy efficiency are heavily dependent on and scaling with the skyrmion diffusion speed: In Brownian token-based computing on the one hand, diffusion is used as propagation mechanism for the skyrmions to search forward paths in token-based computing networks. On the other hand, in Brownian reservoir computing, skyrmion diffusion serves as automatic reset mechanism and is necessary to overcome device imperfections. Even though skyrmion diffusion on the reported time scales[6] has recently been experimentally demonstrated to successfully enable Brownian reservoir computing,[34] a faster operation of

R. Gruber, M. A. Brems, J. Rothörl, T. Sparmann, M. Schmitt, I. Kononenko, F. Kammerbauer, M.-A. Syskaki, P. Virnau, M. Kläui
Johannes Gutenberg-Universität Mainz
Institut für Physik
Staudingerweg 7, 55128 Mainz, Germany
E-mail: mathias.klaeui@magnetism.ch

I. Kononenko
National Academy of Sciences of Ukraine
Institute of Applied Physics
58 Petropavlivska St., Sumy 40000, Ukraine

M.-A. Syskaki
Singulus Technologies AG
Hanauer Landstraße 103, 63796 Kahl am Main, Germany

O. Farago
Biomedical Engineering Department
Ben Gurion University of the Negev
Be'er Sheva 84105, Israel

The ORCID identification number(s) for the author(s) of this article can be found under https://doi.org/10.1002/adma.202208922.

DOI: 10.1002/adma.202208922

such devices or especially processing input signals on shorter time scales—such as for the newly proposed audio recognition[36]—is only enabled by higher skyrmion diffusion speeds. Unless strongly driven, the skyrmion dynamics has been found to be heavily impacted by size-dependent pinning effects that induce a non-flat effective energy landscape.[27,37] Thus, pinning causes non-homogeneous probability densities for skyrmion occurrences,[27] reducing the reliability of conventional skyrmion devices and making device operational properties vary between samples. Thus, pinning leads to unwanted and uncontrolled variations from device to device. Consequently, pinning can impede the functionality of devices relying on deterministic skyrmion motion and has additionally been shown to massively slow down skyrmion diffusion[6] to the detriment of the performance of diffusion-exploiting devices.[9] For skyrmion-based neuromorphic computing, skyrmion pinning of an appropriate strength can be an essential source of non-linearity, though one needs to be able to tune the pinning effect so it appropriately competes with other interactions in the system.[34,38] Hence, there is a clear need for means to control the diffusion and attenuate pinning effects to achieve higher operation reliability and to speed up or even enable specific computations by enhanced diffusion as proposed for pinning-free thermal dynamics.[39]

Periodic excitations of systems have become a topic of major interest recently as periodic modulation can not only vary the properties in time but even stabilize new states epitomized by Floquet states.[40] In magnetic systems, periodic drive even in the classical limit has shown to excite eigenmodes—such as the skyrmion breathing mode in the GHz regime—and parametric pumping can be used to manipulate skyrmions.[41] However, so far the impact on the motion and translational dynamics has not been explored.

In this work, we study how the skyrmion diffusion can be tuned by periodic excitations due to an oscillating out-of-plane magnetic field. In contrast to the well-studied case of static fields,[6,28] we find that we can directly control the effective pinning by applying field oscillations. Therefore, the observed effect can be a key enabler for non-conventional computing schemes. We find specifically that the skyrmion diffusion coefficient can be increased by more than two orders of magnitude at a constant temperature. Unlike other methods to tune skyrmion diffusion by external drives, which employ random sequencing of deterministic excitations,[9] our method does not require to input any external randomness to the system. Instead, we solely rely on deterministic (periodic) excitation in the sub-Hz to kHz regime and exploit the intrinsic system properties. Beyond the drastic increase in the dynamics, we find that qualitatively, the dynamic regime changes from pinning-dominated to approaching free diffusion. Moreover, we observe that during the oscillating field excitation, skyrmions remain stable at field values that lead to much larger and smaller diameters than achievable for stationary field configurations. This observation may lay a foundation for ultrafast skyrmion transport by transiently tuning the size of skyrmions during brief application of spin torques or field gradients to move them.

2. Diffusion Enhanced and Tuned by Magnetic Field Oscillation

We investigate the diffusion of skyrmions in a Ta(4)/$Co_{20}Fe_{60}B_{20}$(0.85)/Ta(0.08)/MgO(2)/HfO_2(4) multilayer stack exhibiting low pinning.[6,27] Layer thicknesses are given in nanometers in parentheses. The skyrmion density is controlled by the nucleation sequence including the out-of-plane (OOP) magnetic field and is kept low to suppress skyrmion–skyrmion interactions. The magnetic contrast is established in real time using Kerr microscopy with blue light and a time resolution of 62.5 ms. From the obtained movies, the skyrmions are detected and trajectories are linked with trackpy.[42] We start by studying the diffusion using our previously established method.[6,28] Then, we compare this diffusion to the dynamics when additionally applying an oscillating OOP field. **Figure 1**a shows

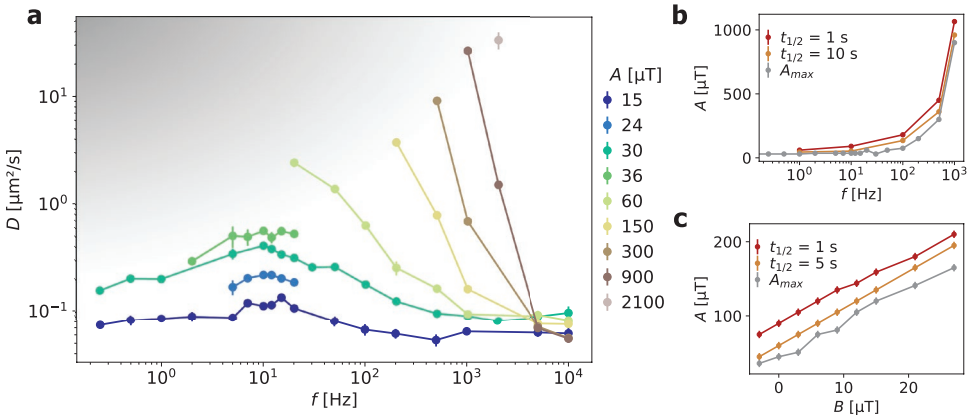

Figure 1. Enhanced skyrmion diffusion and stability in field oscillation. a) The skyrmion diffusion constant D depends on field oscillation frequency f and peak-to-peak amplitude A. Solid lines are guide to the eye along a frequency scan at fixed amplitude. For low frequencies, the maximum applicable field amplitude $A_{max,}$ for which skyrmions do not annihilate, is limited. Therefore, not all amplitudes can be evaluated over the whole frequency range, the inaccessible region is indicated by the gray-shaded area. b) A_{max} (gray) increases with frequency. Higher amplitudes lead to an increasingly fast decay of the number of skyrmions. Amplitudes are shown that correspond to a half-life of 10 (orange) and 1 s (red). c) A_{max} also increases with increasing offset field values (i.e., skyrmion size) while keeping f constant at 100 Hz, as shown by the gray line. Amplitudes leading to half-lives of 5 (orange) and 1 s (red) behave similarly.

how the diffusion coefficient depends on field amplitude and frequency. Generally, larger amplitudes yield a higher diffusion constant. For constant amplitude, however, D increases from the unexcited case up to a peak at $f = (10 \pm 2)$ Hz and decreases again for higher frequencies. By variation of the frequency and amplitude, we can effectively tune the skyrmion diffusion coefficient even at a constant temperature. In particular, we find a maximum increase by a factor of ≈ 330 in the diffusion coefficient comparing excited and unexcited diffusion. And this maximum is currently only limited by the time resolution of our optical detection scheme. As discussed in Note S2 (Supporting Information), such an acceleration in the diffusion can be a key enabler for non-conventional computing by significantly decreasing the mean computation time of, for example, a skyrmion-based microscale Brownian half-adder.[9]

Next, we discuss the mechanism of the diffusion enhancement effect due to size oscillations in the context of skyrmion boundary pinning. Previous investigations have shown (both experimentally and micromagnetically) that the position where a skyrmion is pinned at a fixed external field without applied oscillation is often not favorable when the skyrmion becomes smaller or larger.[27] Thus, when the size of the skyrmion is changed by an out-of-plane field,[6,27,43] the effective pinning energy landscape changes as well and new pinning positions become favorable.[27] We note that the change in size due to field oscillations up to the kHz regime is qualitatively different from the skyrmion breathing mode,[41] possibly leading to only segments of the skyrmion boundary moving to expand the skyrmion.[27]

During the field oscillation, the skyrmion with its varying size experiences a variety of different effective energy landscapes, some of which may make it easier for the skyrmion to escape from its current position by thermal diffusion, and thus effectively depin the skyrmion. We note that the diffusion enhancement is generally larger when the oscillation amplitude is larger. We attribute this effect to a stronger variation of the skyrmion size making a broader range of energy landscapes accessible such that skyrmions become more likely to experience a low-pinning landscape. However, note that we cannot apply oscillations of arbitrary amplitude for every frequency due to skyrmions decaying differently rapidly. This stability effect is discussed in detail in the following Section 3. Sometimes, during the increased-size half-cycle, the boundary of the skyrmion may stick to a distant strong boundary pinning site and then contract toward this pinning site and thereby also increase diffusion. However first, the latter effect cannot explain why the diffusion coefficient decreases in the high-frequency limit. Second, we observe an increase in diffusion even if the skyrmion size during the oscillation never exceeds a given static size. In particular, the diffusion coefficient at a static field of 21 μT is $D = (0.105 \pm 0.006)$ μm^2 s^{-1}, which is smaller than the diffusion coefficient for an oscillating field ≈ 30 μT with peak-to-peak amplitude of 15 μT, which is $D = (0.121 \pm 0.004)$ μm^2 s^{-1} even though the field is never reduced to values < 21 μT. This effect can also not be explained solely by expansion and pinning of the skyrmion boundary but requires consideration of thermal effects as discussed above.

Moreover, the change in diffusion depends clearly on the oscillation frequency. In the low-frequency limit, the size-change-induced depinning is on the same timescale as the thermal depinning; therefore, the resulting diffusion coefficient approaches the unexcited case (limit toward 0 Hz). Therefore, those very low frequencies are in general not able to cause significant diffusion enhancement. In the high-frequency limit, the time interval during which the skyrmion remains in a possible low-pinning energy landscape is too short to significantly move away from its current position by thermal diffusion. It remains close to the position where it has been pinned and thus, high frequencies are not suitable to cause effective depinning either. In between these two limits, there exists a regime where, due to the change in size, the skyrmion temporarily is in a low-pinning energy landscape and can diffuse away from the position where it is pinned when it has a different size. Imagine—without loss of generality—the skyrmion is currently at a position where pinning is strong at small sizes but weak at much larger sizes. Assume that during a certain time interval as part of the field oscillation, the skyrmion is large enough such that it feels only weak pinning. Then, it thermally diffuses to a position where large skyrmions are pinned strongly, but very small skyrmions are pinned weakly. When the size is reduced, the skyrmion is weakly pinned and can diffuse again to a position where small skyrmions are pinned strongly. Thereby, the total diffusion is effectively increased.

To corroborate the proposed general concept of depinning of domain walls due to field excitations, we additionally analyze stripe domains in oscillating magnetic fields. We find that in analogy to the case of skyrmions, the stripes (or more specifically, the domain walls at their boundaries) move more for applied excitations, in particular for higher field amplitudes. Kerr microscopy data visualizing the effect can be found in Figure S2 (Supporting Information). To stress the scope of the effect beyond the specific system presented here, we furthermore analyze the influence of field excitations on various skyrmion systems. Plots similar to the one in Figure 1a are presented in the Supporting Information for a system with comparable skyrmion density but stronger pinning (Figure S3a, Supporting Information) as well as for a very dense skyrmion system (Figure S3b, Supporting Information) showing qualitatively consistent behavior. We note that in confined geometries such as wires, the size variations of the skyrmions due to field oscillations may be limited by the device edge effects. In Figure S3c (Supporting Information) however, we show that even in a wire geometry with a width of 1.8 skyrmion diameters, we can still enhance the diffusion by a factor of nearly 100. Hence, the mechanism of periodic field excitations is not strongly suppressed by geometrical confinements. Therefore, it appears widely applicable to as well as useful for a variation of different skyrmion systems and for several devices based on skyrmion diffusion in different geometries.

3. Skyrmion Stability in Oscillating Field

Next, we discuss the effect of the magnetic field oscillations on the stability of the skyrmions. In response to the magnetic field, the skyrmions vary their size during the oscillations. At constant external fields, we find that in our sample, skyrmions are only existing as a stable phase in the field range from

21 to 63 μT. For higher fields, skyrmions become too small and annihilate on time scales of <1 s whereas for lower fields, skyrmions start expanding into stripes as previously observed.[31] When applying field oscillations, we choose a field offset that is inside this field range. We note however that we can apply field oscillation amplitudes of the order of milliteslas, hence orders of magnitude beyond what is applicable in the static case, when going to frequencies in the kHz regime: for low oscillation frequencies, the maximum applicable amplitude A_{max} without leading to a significant amount of skyrmions annihilations is coinciding well with the field region at which skyrmions are stable at static fields. However, beyond 10 Hz, A_{max} increases clearly with frequency. For frequencies in the kilohertz regime, even amplitudes of hundreds of microteslas can be applied even though the sample reaches saturation at 150 μT already in the static case. In Figure 1b, A_{max} as well as the field amplitudes corresponding to half-lives of 10 and 1 s are shown as function of the frequency.

We furthermore find that A_{max} is dependent on the offset field. Figure 1c shows A_{max} as well as the field amplitudes corresponding to half-life times of 5 and 1 s for varying offset fields. In particular, A_{max} increases with increasing offset. Thus, A_{max} increases with the average skyrmion size. We find that large skyrmions become stripe-like when the field is decreased to values <21 μT. In contrast, when starting with the smallest stable skyrmions and increasing the magnetic field to values >63 μT, the skyrmions annihilate.

We conclude that skyrmions start annihilating when their size drops below a threshold value. The skyrmion annihilation process is thermally activated and small skyrmions below this size threshold are not stable anymore but still require additional energy to overcome the topological stabilization energy barrier to annihilate. This leads to a finite probability of annihilation and an exponential decay of the number of skyrmions. Hence, the speed at which the skyrmions decay depends on the time interval during which the size is below the threshold for stability. However, the fraction of a time-span for which the field is below a certain value depends on the amplitude only, not on the frequency. Therefore, we conclude that the skyrmion permanently adjusts itself to the non-flat energy landscape leading to a multi-step process approaching the small skyrmion state, such that the long-term decay rate is indeed dependent on the oscillation period time. Hence, the enhanced stability of skyrmions in field oscillation is a consequence of pinning effects.

Potentially, the ability to briefly change the size of skyrmions beyond their static stability limits is promising for ultrafast skyrmion motion. As the skyrmion velocity depends on its size, one can enhance the size of a skyrmion briefly while generating spin-torques by injecting a current pulse to induce much faster motion than accessible within the static stability limits.

4. Effective Reduction of Pinning Effects

For the case of excitation with an amplitude of A = 30 μT we experimentally observe a maximum diffusion constant increase of ≈300% compared to the case without excitation. In contrast, the diffusion we would obtain by keeping the skyrmion small all the time by statically applying the lower bound size of the field oscillation is only 31% higher than the diffusion at the offset field. Moreover, increased diffusion based on the non-linear dependence of the dissipation tensor on the skyrmion size derived by Schütte et al.[39] can only account for an increase of 1.6%. The corresponding calculation as well as the experimentally determined relations between magnetic field, skyrmion size, and diffusion constant can be found in Note S1 and Figure S1 (Supporting Information). Therefore, we conclude that the main reason for the enhanced diffusion cannot be the non-linear size dependence of the dissipation tensor. Instead, we propose that the periodic size change effectively reduces the skyrmion pinning. Recently, a strong size dependence of skyrmion pinning has been reported,[27] allowing one to attenuate the influence of certain pinning sites by changing the skyrmion size. Finally, we note that skyrmions have been found to exhibit hopping-like diffusion in a non-flat energy landscape due to the pinning effect[6,27] in contrast to the expected free diffusion of Brownian particles.[44]

Similar to our analysis in the previous work,[27] we ascertain the spatially resolved occurrence map with and without excitation as described in the Experimental Section. We observe in **Figure 2**a,c that with applied oscillating field, the occurrence map is significantly more homogeneous indicating an overall flatter energy landscape and thus lower effective pinning. At a constant field of 30 μT, large parts of the sample are never visited within 10 min of measurement. Utilizing a field oscillation of 2100 μT peak-to-peak amplitude at 2 kHz however, we can tune the system such that almost every pixel of the video hosts the center of a skyrmion a least once within the same time. The data shown in Figure 2a,c are limited to the occurrences within 10 min for both plots to allow for comparison. The full gathered statistics for the unexcited case in Figure 2a as well as the corresponding spatially resolved energy landscapes are provided in Figures S4 and S5 (Supporting Information), respectively. Kerr microscopy data corresponding to the unexcited and excited case are shown in Videos S1 and S2 (Supporting Information), respectively. We conclude that by oscillation of the out-of-plane field, we can strongly attenuate the effective skyrmion pinning and enable a rather uniform movement of skyrmions anywhere in the sample.

The ability to tune the pinning energy landscape is of importance for skyrmion-based neuromorphic computing such as reservoir computing[34,38] since pinning is a valuable source of the required non-linearity of the system but must be of the order of other interactions in the system for efficient operation. Moreover, the effectively flattened energy landscape with more isotropic skyrmion movement reduces variations between equivalent devices and thus increases or even ensures the operation reliability but also the potential for applications.

Figure 2b,d displays two sets of trajectories comparing the unexcited case with the amplitude-frequency pair from Figure 1a yielding the highest diffusion. We find that with increasing amplitude of oscillation, the diffusion becomes less hopping-like and approaches isotropic free diffusion. Note that the scales of Figure 2b,d is different as more strongly diffusing skyrmions cover more of the sample area within the same time.

This now calls for a final analysis, where we check whether there is not just a quantitative but really a qualitative difference in the type of diffusive motion as discussed above. To

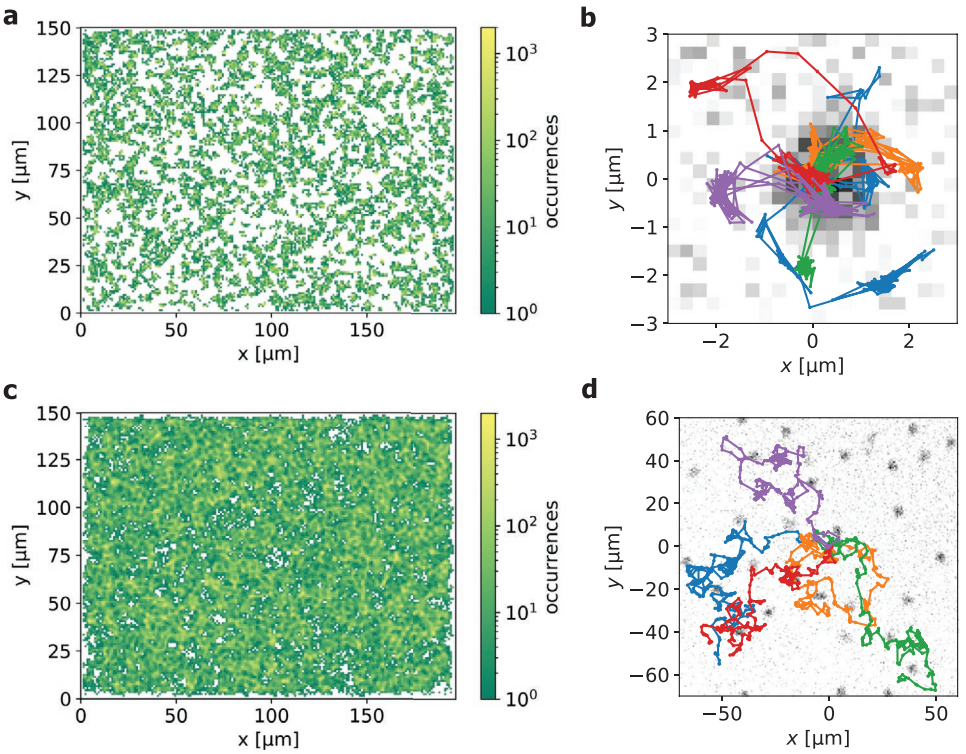

Figure 2. Skyrmion movement with and without periodic field excitation. a) The positions of skyrmion occurrences at a static field of 30 µT over 10 min are found at distinct places while large parts of the sample are never visited. b) Example trajectories with respect to the coordinate origin of the case in (a) show a clear hopping behavior. Each color represents one skyrmion. The grayscale background depicts a single Kerr microscopy frame image of one of those skyrmions at the coordinate origin. c) Analogously, the occurrence histogram—for the same time interval as in (a)—as well as d) example trajectories are evaluated for a magnetic field oscillating ≈ 30 µT with a frequency of 2 kHz and a peak-to-peak amplitude of 2100 µT. During the excitation, the skyrmions travel over larger distances and explore nearly the whole sample. As in (b), a single Kerr microscopy frame image with one of the respective skyrmions in the center is used as grayscale background.

understand and quantify the difference between the dynamics with and without excitation, we analyze the distributions of the skyrmion displacements after 2 s to gauge the system's relative proximity to the free diffusion limit. In a classical freely diffusing system, each component of the displacement should be Gaussian distributed. The absolute displacement should consequently follow a Rayleigh distribution

$$p(\Delta x) \sim \Delta x\, e^{-\frac{\Delta x^2}{2\sigma^2}} \tag{1}$$

Figure 3a,b shows the displacement in *x*-direction and the absolute displacement, respectively, after 2 s as histograms for the excited case established in Figure 2c, which corresponds to a magnetic field oscillating around an offset value = 30 µT with a frequency of 2 kHz and a peak-to-peak amplitude of 2100 µT. We find that the measured *x*-displacement distribution is composed of two contributions: The sharp peak around zero displacement (labeled as A) reflects the marginal movement in the vicinity of pinning sites, for example, in a harmonic well. The wider part (label B) corresponds to the quasi-free motion leading to larger displacements and is the dominating component here. Since both contributions are expected to exhibit random motion, we fit a sum of two Gaussians to the distribution in Figure 3a. Because the two regimes A and B are separated such that pinned skyrmions are found in regime A for both *x* and *y* displacement (while free-like motion correspondingly leads to regime B for both dimensions), we fit the 2D case in Figure 3b with a sum of two Rayleigh distributions accounting for each A and B. The fitted distributions are clearly in good agreement to the observed displacements, endorsing the random walk nature of the skyrmions for both the motion within pinning sites and the quasi-freely diffusing regime. That is, we indeed see a qualitatively different, free-like type of diffusion—in contrast to the hopping motion observed in previous investigations.[6,28] The small additional peak present at displacements of ≈ 4 µm in Figure 3b is a consequence of skyrmions hopping from one pinning site to a close neighboring pinning site once. It arises as soon as the neighboring pinning site is in reach of the skyrmion boundary during the size oscillation. We observe that the peak position is related to the skyrmion size and the characteristic distances between pinning sites, which have been discovered previously as a consequence of the sample fabrication.[27] Quantitatively, the peak is of minor importance and not generic but sample-specific and therefore omitted in the fit. Furthermore, we note that a small net motion component due to a slight field gradient shifts the regime B of the *x*-displacement slightly to negative values. For the unexcited case from Figure 2a, we observe in comparison that the peak around zero displacement corresponding to movement

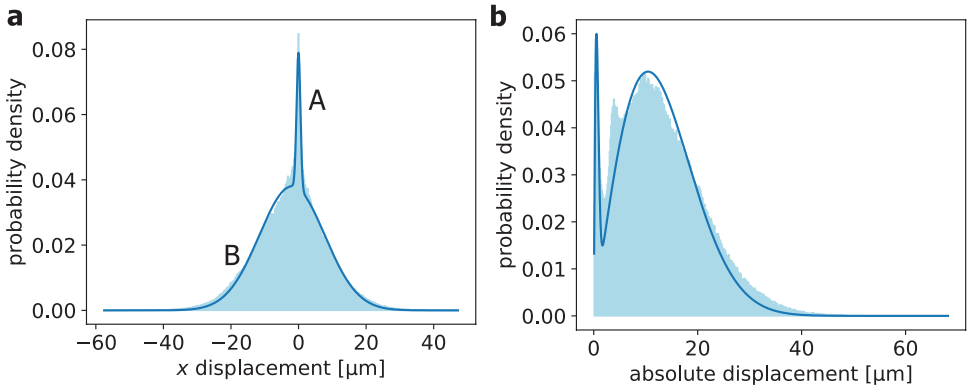

Figure 3. Skyrmion displacement distributions. a) The *x*-components and b) absolute values of skyrmion displacements within 2 s under a field oscillation at 2 kHz with a peak-to-peak amplitude of 2100 µT around an offset field of 30 µT are shown as histogram in light blue. The peak around zero displacement (labeled as A) represents movements within the pinning site whereas the wider distribution (labeled as B) corresponding to further displacements belongs to the quasi-free diffusive behavior. The shift of the wider distribution B in (a) toward negative values reveals a slight net motion due to a small field gradient throughout the sample. In good agreement with the experimental data, a sum of two Gaussian distribution accounting for each A and B is fitted to the 1D case in (a) as this behavior is expected for Brownian-like random walk independently for both regimes. Analogously, a sum of two Rayleigh distributions is fitted as the 2D equivalent in (b). The small additional peak at displacements ≈ 4 µm arises from skyrmions hopping to close neighboring pinning sites.

within pinning sites dominates whereas hopping between pinning sites leads to only slightly larger displacements. The corresponding plots are provided in Figure S6 (Supporting Information). Note that the displacement distributions in Figure 3 and Figure S6 (Supporting Information) are taken for the same, finite time scale and the component-wise displacement distribution will converge to a Gaussian in both in the limit of infinite timescales. For the strongly excited case shown in Figure 3, we conclude however that the observed diffusion is governed by a diffusive motion close to free diffusion leading to large displacements.

5. Conclusion

We demonstrate a mechanism to tune the diffusive dynamics of skyrmions in a magnetic thin film by an oscillating magnetic field. We show that we can enhance the diffusion by two orders of magnitude, limited only by the time resolution limit of our imaging technique and with the potential to drastically speed up skyrmion-based non-conventional computing methods originating from Brownian computing and reservoir computing paradigms. When the diffusion is enhanced, we find that the energy landscape becomes effectively flattened corresponding to a reduction of the effective pinning. In accordance with the recently reported strong size dependence of the pinning, we can conclude that the effectiveness of pinning sites is strongly reduced as the skyrmions undergo significant size changes, which compensates for sample specific pinning landscapes and hence suppresses undesirable effects resulting from device-to-device variations. In the analysis of the dynamics, we can identify a qualitative difference: when strongly excited, the skyrmion diffusion is dominated by Brownian motion approaching free diffusion while in the case of no or weak excitation, hopping displacements within the pinning site are dominating. During the field oscillation, we find that skyrmions remain stable even when exposed to magnetic fields at which they immediately annihilate without oscillation. The enhanced stability is also traced back to pinning mediated effects and can be a key enabler to tune skyrmion properties by size changes and thus enhance operation reliability of skyrmion devices. Therefore, our findings present a method to tune and drastically enhance speed and operation reliability of skyrmion-based non-conventional computing devices and open up an unexplored gateway to ultrafast and efficient skyrmion transport.

6. Experimental Section

Sample Characterization: The investigated material was a Ta(4)/$Co_{20}Fe_{60}B_{20}$(0.85)/Ta(0.08)/MgO(2)/HfO_2(4) multilayer stack with layer thicknesses given in nanometers in the parentheses. The piece of 10 × 10 mm^2 size was deposited with a *Singulus Rotaris* magnetron sputtering tool at a base pressure of 3 × 10^{-8} mbar. Thereby, the layer thicknesses were reproducible with an accuracy of better than 0.01 nm and the surface roughness was found to be <1 nm. The interface between the ferromagnetic $Co_{20}Fe_{60}B_{20}$(0.85) and the MgO(2) causes the sample to exhibit perpendicular magnetic anisotropy, which was tuned by the Ta(0.08) interlayer.[6] The saturation magnetization (M_S = (0.46 ± 0.02) MA m^{-1}) and effective anisotropy constant (K_{eff} = (41 ± 3) kJ m^{-3}) were determined from a hard axis hysteresis loop with anisotropy field B_S = (179 ± 10) mT using a superconducting quantum interference device. From this, a magnetic domain wall width of Δ = (16±1) nm was calculated for a typical exchange stiffness of A = (10 ± 1) pJ m^{-1}.[6] The Ta(4)/$Co_{20}Fe_{60}B_{20}$(0.85) interface provides interfacial DMI that was measured for similar stacks to be D ≈ (0.30 ± 0.08) mJ m^{-2}.[6,28,45] The HfO_2(4) was used as capping to prevent the sample from oxidization while still allowing for good imaging contrast due to being optically transparent. The out-of-plane hysteresis loop of the used sample is shown in Figure S7 (Supporting Information). The topologically nontrivial structure of the observed skyrmionic bubbles was confirmed by studying the displacements using spin-orbit torques as well as by evaluating the spin structure in micromagnetic simulations, proving that indeed chiral skyrmions are studied.[6,27,28]

Measurement Setup: Magnetic contrast was established using the polar magneto-optical Kerr effect (MOKE) in a commercially available Kerr microscope from evico magnetics GmbH. Magnetic fields in in-plane (IP) as well as out-of-plane (OOP) direction can be applied by

separate and perpendicularly aligned electromagnetic coils. The OOP magnet was custom-made and constructed to generate small fields with sub-microtesla precision. Directly on top of the coil, there was a Peltier element for sample temperature regulation, where a Pt100 heat sensor was used to observe the actual temperature directly next to the sample with accuracy and stability better than 0.1 K. The whole setup was housed additionally in a thermally stabilized flow box. Magnetic structures and hystereses were characterized between 315 and 330 K. For the diffusion measurements, the sample temperature was kept constant at 319.0 K, where skyrmions were found in various densities and stable between 21 and 63 μT OOP field and exhibiting thermal diffusion. The magnetic field values were calibrated by a sensitive Hall probe and external fields were corrected by the hysteresis offset. The OOP field was found to be constant and reproducible with a gradient at the sample position of $<0.01\ \mu T\ \mu m^{-1}$. For the field oscillation, the OOP coil was supplied by an Agilent 33250A Arbitrary Waveform Generator and the current through the coil was checked with an oscilloscope. Data was acquired by a CCD camera as gray-scale videos with a field of view of $200 \times 150\ \mu m^2$ at 16 frames per second with a time resolution of 62.5 ms.

The skyrmions were nucleated at a fixed OOP field by applying a saturating IP field pulse such that skyrmions form as stable state when the IP field was switched off and the spins relax into OOP domains. The number of skyrmions (i.e., the skyrmion density) was controlled by the IP and OOP field value. The skyrmion size was directly tuned by the OOP field at constant temperature.

Skyrmion Detection and Tracking: From the grayscale videos, the frames were preprocessed and skyrmions were detected using the trackpy package.[42] The detection was performed by a 2D Gaussian fit into local intensity maxima exceeding threshold values for both maximum intensity values, intensity peak size, and integrated intensity within the fit region. The magnetic contrast between opposite magnetized domains yields the required significant intensity edges. The contrast was further enhanced by applying background subtraction with respect to a saturated state. Due to the detection fit over a large pixel number and beyond the skyrmion core, the skyrmion center can be determined with accuracy below the optical resolution of the microscope (≈300 nm) as previously reported.[27] Originating from the tracking procedure, the skyrmion size refers to the radius of gyration of the fitted Gaussian kernel.

All measurements were performed in one run and at the same position on the sample. Since the sample size exceeds the field of view by more than one order of magnitude, the skyrmion system was treated as infinite allowing boundary effects to be neglected. However, one could still map positions between the single videos due to topographic defects at the sample surface and the performed background subtraction with a static background image. From the subtracted images, it was deduced that the sample drift throughout the measurement series was <300 nm, which means that indeed all measurements were performed at the same sample position.

Investigating Skyrmion Dynamics—Diffusion Coefficients, Occurrence Maps, and Displacement Distributions: The diffusion coefficients in Figure 1 have been calculated based on the skyrmion trajectories using the relation $\langle[\Delta x(\Delta t)]^2\rangle = 2dD\Delta t$. Here, $[\Delta x(\Delta t)]^2$ is the squared spatial displacement during the time Δt, $d = 2$ is the dimension of the system and D is the diffusion coefficient. Angled brackets indicate the average over the individual skyrmions as well as over different sections of each trajectory with length Δt (sliding window method). The diffusion coefficient D was calculated by fitting the well-sampled regions of $\langle[\Delta x(\Delta t)]^2\rangle$ with $2dD\Delta t$ for 3 to 5 videos of 1 min length for each amplitude-frequency pair and averaging over the values for each video. The uncertainty of the diffusion coefficient was estimated using the standard error of the mean.

Occurrence maps were calculated from the tracked skyrmion center positions in videos with equal experimental conditions. Tracked positions were put into bins with a bin width of 1 μm resulting in an occurrence landscape that was plotted logarithmically for readability. Some bins were never visited by a skyrmion leading to incomplete sampling of the landscape. To improve comparability between experiments with and without applied field, the number of points in both maps were kept equal by using only part of the statistics recorded for skyrmions without an applied field.

Distributions of displacements were calculated by determining the displacement of a skyrmion after $\Delta t = 2$ s. As for the diffusion constant, the sliding window method and multiple videos were used to improve the statistics. The values were then divided into equally distributed bins in a histogram. While the instantaneous velocities were experimentally inaccessible, the distributions of displacements to gauge the two systems' relative proximity to the free diffusion limit on the same timescale could still be compared. The shape of this distribution depends on the time Δt, soa time was chosen that was long enough to contain both, movement between pinning sites as well as skyrmions staying at their place.

Supporting Information

Supporting Information is available from the Wiley Online Library or from the author.

Acknowledgements

The authors are grateful to the Deutsche Forschungsgemeinschaft (DFG, German Research Foundation) for funding this research: Project number #403502522-SPP 2137 Skyrmionics, SFB TRR 173 Spin+X (project A01 #268565370 and project B12 #268565370), SFB TRR 146 (project #233630050). The authors further acknowledge funding from TopDyn, and this project has furthermore received funding from the European Union's Horizon 2020 research and innovation programme under grant no. 863155 (s-Nebula), grant no. 856538 (3D MAGIC) and under the Marie Skłodowska-Curie grant agreement no. 860060 (MagnEFi). M.B. was supported by a doctoral scholarship of the Studienstiftung des deutschen Volkes.

Open access funding enabled and organized by Projekt DEAL.

Conflict of Interest

The authors declare no conflict of interest.

Author Contributions

R.G. prepared the measurement setup and performed the Kerr microscopy measurements with the help of T.S.; I.K., F.K., and M.A.S. fabricated the multilayer sample. R.G., M.B., and J.R. evaluated the experimental data and prepared the manuscript supported by P.V. and M.K.; O.F. helped with the interpretation of the results. J.R., M.B., and M.S. provided the theoretical calculations. The study was supervised by M.K. and P.V.; all authors commented on the manuscript.

Data Availability Statement

The data that support the findings of this study are available from the corresponding author upon reasonable request.

Keywords

diffusion, non-conventional computing, pinning, skyrmions, spintronics

Received: September 27, 2022
Revised: January 30, 2023
Published online: March 18, 2023

[1] A. Bogdanov, A. Hubert, *J. Magn. Magn. Mater.* **1994**, *138*, 255.
[2] S. Mühlbauer, B. Binz, F. Jonietz, C. Pfleiderer, A. Rosch, A. Neubauer, R. Georgii, P. Böni, *Science* **2009**, *323*, 915.
[3] W. Jiang, G. Chen, K. Liu, J. Zang, S. G. E. te Velthuis, A. Hoffmann, *Phys. Rep.* **2017**, *704*, 1.
[4] K. Everschor-Sitte, J. Masell, R. M. Reeve, M. Kläui, *J. Appl. Phys.* **2018**, *124*, 240901.
[5] P. Huang, T. Schönenberger, M. Cantoni, L. Heinen, A. Magrez, A. Rosch, F. Carbone, H. M. Rønnow, *Nat. Nanotechnol.* **2020**, *15*, 761.
[6] J. Zázvorka, F. Jakobs, D. Heinze, N. Keil, S. Kromin, S. Jaiswal, K. Litzius, G. Jakob, P. Virnau, D. Pinna, K. Everschor-Sitte, L. Rózsa, A. Donges, U. Nowak, M. Kläui, *Nat. Nanotechnol.* **2019**, *14*, 658.
[7] X. Zhang, M. Ezawa, Y. Zhou, *Sci. Rep.* **2015**, *5*, 9400.
[8] D. Pinna, F. Abreu Araujo, J.-V. Kim, V. Cros, D. Querlioz, P. Bessiere, J. Droulez, J. Grollier, *Phys. Rev. Appl.* **2018**, *9*, 064018.
[9] M. A. Brems, M. Kläui, P. Virnau, *Appl. Phys. Lett.* **2021**, *119*, 132405.
[10] A. Fert, V. Cros, J. Sampaio, *Nat. Nanotechnol.* **2013**, *8*, 152.
[11] S. Parkin, S.-H. Yang, *Nat. Nanotechnol.* **2015**, *10*, 195.
[12] X. Zhang, G. P. Zhao, H. Fangohr, J. P. Liu, W. X. Xia, J. Xia, F. J. Morvan, *Sci. Rep.* **2015**, *5*, 7643.
[13] X. Yu, F. Kagawa, S. Seki, M. Kubota, J. Masell, F. S. Yasin, K. Nakajima, M. Nakamura, M. Kawasaki, N. Nagaosa, Y. Tokura, *Nat. Commun.* **2021**, *12*, 5079.
[14] Y. Chen, Z. Li, Z. Zhou, Q. Xia, Y. Nie, G. Guo, *J. Magn. Magn. Mater.* **2018**, *458*, 123.
[15] F. Büttner, C. Moutafis, M. Schneider, B. Krüger, C. M. Günther, J. Geilhufe, C. v. K. Schmising, J. Mohanty, B. Pfau, S. Schaffert, A. Bisig, M. Foerster, T. Schulz, C. a. F. Vaz, J. H. Franken, H. J. M. Swagten, M. Kläui, S. Eisebitt, *Nat. Phys.* **2015**, *11*, 225.
[16] Y. Liu, N. Lei, C. Wang, X. Zhang, W. Kang, D. Zhu, Y. Zhou, X. Liu, Y. Zhang, W. Zhao, *Phys. Rev. Appl.* **2019**, *11*, 014004.
[17] X. Wang, W. L. Gan, J. C. Martinez, F. N. Tan, M. B. A. Jalil, W. S. Lew, *Nanoscale* **2018**, *10*, 733.
[18] F. Jonietz, S. Mühlbauer, C. Pfleiderer, A. Neubauer, W. Münzer, A. Bauer, T. Adams, R. Georgii, P. Böni, R. A. Duine, K. Everschor, M. Garst, A. Rosch, *Science* **2010**, *330*, 1648.
[19] X. Z. Yu, N. Kanazawa, W. Z. Zhang, T. Nagai, T. Hara, K. Kimoto, Y. Matsui, Y. Onose, Y. Tokura, *Nat. Commun.* **2012**, *3*, 988.
[20] S. Woo, K. Litzius, B. Krüger, M.-Y. Im, L. Caretta, K. Richter, M. Mann, A. Krone, R. M. Reeve, M. Weigand, P. Agrawal, I. Lemesh, M.-A. Mawass, P. Fischer, M. Kläui, G. S. D. Beach, *Nat. Mater.* **2016**, *15*, 501.
[21] S. Komineas, N. Papanicolaou, *Phys. Rev. B* **2015**, *92*, 064412.
[22] J. Iwasaki, M. Mochizuki, N. Nagaosa, *Nat. Commun.* **2013**, *4*, 1463.
[23] A. Hrabec, J. Sampaio, M. Belmeguenai, I. Gross, R. Weil, S. M. Chérif, A. Stashkevich, V. Jacques, A. Thiaville, S. Rohart, *Nat. Commun.* **2017**, *8*, 15765.
[24] K. Litzius, I. Lemesh, B. Krüger, P. Bassirian, L. Caretta, K. Richter, F. Büttner, K. Sato, O. A. Tretiakov, J. Förster, R. M. Reeve, M. Weigand, I. Bykova, H. Stoll, G. Schütz, G. S. D. Beach, M. Kläui, *Nat. Phys.* **2017**, *13*, 170.
[25] K. Litzius, J. Leliaert, P. Bassirian, D. Rodrigues, S. Kromin, I. Lemesh, J. Zazvorka, K.-J. Lee, J. Mulkers, N. Kerber, D. Heinze, N. Keil, R. M. Reeve, M. Weigand, B. Van Waeyenberge, G. Schütz, K. Everschor-Sitte, G. S. D. Beach, M. Kläui, *Nat. Electron.* **2020**, *3*, 30.
[26] R. Juge, S.-G. Je, D. S. de Chaves, L. D. Buda-Prejbeanu, J. Peña-Garcia, J. Nath, I. M. Miron, K. G. Rana, L. Aballe, M. Foerster, F. Genuzio, T. O. Mentes, A. Locatelli, F. Maccherozzi, S. S. Dhesi, M. Belmeguenai, Y. Roussigné, S. Auffret, S. Pizzini, G. Gaudin, J. Vogel, O. Boulle, *Phys. Rev. Appl.* **2019**, *12*, 044007.
[27] R. Gruber, J. Zázvorka, M. A. Brems, D. R. Rodrigues, T. Dohi, N. Kerber, B. Seng, M. Vafaee, K. Everschor-Sitte, P. Virnau, M. Kläui, *Nat. Commun.* **2022**, *13*, 3144.
[28] N. Kerber, M. Weißenhofer, K. Raab, K. Litzius, J. Zázvorka, U. Nowak, M. Kläui, *Phys. Rev. Appl.* **2021**, *15*, 044029.
[29] T. Nozaki, Y. Jibiki, M. Goto, E. Tamura, T. Nozaki, H. Kubota, A. Fukushima, S. Yuasa, Y. Suzuki, *Appl. Phys. Lett.* **2019**, *114*, 012402.
[30] Y. Jibiki, M. Goto, E. Tamura, J. Cho, S. Miki, R. Ishikawa, H. Nomura, T. Srivastava, W. Lim, S. Auffret, C. Baraduc, H. Bea, Y. Suzuki, *Appl. Phys. Lett.* **2020**, *117*, 082402.
[31] M. Goto, H. Nomura, Y. Suzuki, *J. Magn. Magn. Mater.* **2021**, *536*, 167974.
[32] J. Lee, F. Peper, S. D. Cotofana, M. Naruse, M. Ohtsu, T. Kawazoe, Y. Takahashi, T. Shimokawa, L. B. Kish, T. Kubota, *Int. J. Unconv. Comput.* **2016**, *12*, 341.
[33] R. Ishikawa, M. Goto, H. Nomura, Y. Suzuki, *Appl. Phys. Lett.* **2021**, *119*, 072402.
[34] K. Raab, M. A. Brems, G. Beneke, T. Dohi, J. Rothörl, F. Kammerbauer, J. H. Mentink, M. Kläui, *Nat. Commun.* **2022**, *13*, 6982.
[35] K. Wang, Y. Zhang, V. Bheemarasetty, S. Zhou, S.-C. Ying, G. Xiao, *Nat. Commun.* **2022**, *13*, 722.
[36] R. Msiska, J. Love, J. Mulkers, J. Leliaert, K. Everschor-Sitte, arXiv:2209.13946, **2022**.
[37] C. Reichhardt, C. J. O. Reichhardt, M. V. Milošević, *Rev. Mod. Phys.* **2022**, *94*, 035005.
[38] D. Pinna, G. Bourianoff, K. Everschor-Sitte, *Phys. Rev. Appl.* **2020**, *14*, 054020.
[39] C. Schütte, J. Iwasaki, A. Rosch, N. Nagaosa, *Phys. Rev. B* **2014**, *90*, 174434.
[40] T. Oka, S. Kitamura, *Annu. Rev. Condens. Matter Phys.* **2019**, *10*, 387.
[41] M. Lonsky, A. Hoffmann, *APL Mater.* **2020**, *8*, 100903.
[42] D. B. Allan, T. Caswell, N. C. Keim, C. M. van der Wel, soft-matter/trackpy: Trackpy v0.5.0, Zenodo: 4682814, **2021**.
[43] X. S. Wang, H. Y. Yuan, X. R. Wang, *Commun. Phys.* **2018**, *1*, 31.
[44] R. Brown, *Philos. Mag.* **1828**, *4*, 161.
[45] N. Kerber, D. Ksenzov, F. Freimuth, F. Capotondi, E. Pedersoli, I. Lopez-Quintas, B. Seng, J. Cramer, K. Litzius, D. Lacour, H. Zabel, Y. Mokrousov, M. Kläui, C. Gutt, *Nat. Commun.* **2020**, *11*, 6304.